BNL-108117-2015-JA

Application of the Hartmann-Tran profile to precise experimental data sets of $^{12}C_2H_2$

D. Forthomme[a], M. J. Cich[b], S. Twagirayezu[a], G. E. Hall[a], T. J. Sears[a,b,*]

[a] *Chemistry Department, Brookhaven National Laboratory, Building 555A, P.O Box 5000, Upton, New York 11973, USA*
[b] *Chemistry Department, Stony Brook University, Stony Brook, New York 11794, USA*

Abstract

Self- and nitrogen-broadened line shape data for the $P_e(11)$ line of the $\nu_1 + \nu_3$ band of acetylene, recorded using a frequency comb-stabilized laser spectrometer, have been analyzed using the Hartmann-Tran profile (HTP) line shape model in a multispectrum fitting. In total, the data included measurements recorded at temperatures between 125 K and 296 K and at pressures between 4 and 760 Torr. New, sub-Doppler, frequency comb-referenced measurements of the positions of multiple underlying hot band lines have also been made. These underlying lines significantly affect the $P_e(11)$ line profile at temperatures above 240 K and poorly known frequencies previously introduced errors into the line shape analyses. The behavior of the HTP model was compared to the quadratic speed dependent Voigt profile (QSDVP) expressed in the frequency and time domains. A parameter uncertainty analysis was carried out using a Monte Carlo method based on the estimated pressure, transmittance and frequency measurement errors. From the analyses, the $P_e(11)$ line strength was estimated to be $1.2014(50)\times10^{-20}$ in cm.molecule^{-1} units at 296K with the standard deviation in parenthesis. For analyzing these data, we found a reduced form of the HTP, equivalent to the QSDVP, was most appropriate because the additional parameters included in the full HTP were not well determined. As a supplement to this work, expressions for analytic derivatives and a lineshape fitting code written

*Corresponding author
Email address: sears@bnl.gov (T. J. Sears)

in Matlab for the HTP, are available.

Keywords: Lineshape modeling, acetylene, C_2H_2, frequency comb referenced spectroscopy, HTP

---

1. Introduction

The Voigt profile (VP) is the standard lineshape model used in high resolution spectroscopy databases for its simplicity and its fast computation time. However, with the ever increasing sensitivity and accuracy of measurement techniques, more subtle effects on the experimental data are now commonly observed. The VP does not account for second order effects in the lineshape such as the speed dependence of the relaxation rate[1] or the collisional narrowing[2]. Particularly at low to moderate pressures, attempts to model measured lineshapes with a VP typically leaves a "w" shaped residual, associated with the narrowing that is not represented in the VP[3]. A wide variety of models of various degrees of complexity have been proposed in an attempt to account for these deviations. Examples include the speed dependent Voigt (SDV)[4, 5], the Galatry[3, 6] and Rautian[3, 7] profiles obtained assuming soft and hard collisions respectively, and profiles using the Keilson-Storer function for velocity changes[8, 9] to cite just a few.

In order to improve the quality and utility of the high resolution spectroscopic databases, an IUPAC (International Union of Pure and Applied Chemistry) task group has recommended[10] the adoption of the Hartmann-Tran profile (HTP) as the new standard lineshape model. The HTP, also referred to as partially Correlated quadratic Speed-Dependent Hard Collision Profile (pCqSDHCP)[11] or partially Correlated quadratic Speed- Dependent Nelkin-Ghatak Profile (pCqSDNGP)[12], has the advantage of incorporating both the speed dependence of the relaxation rate and the velocity changing collision effects in a model that is very fast to compute, while maintaining the physical meaning of the parameters[11, 13, 14]. Other more sophisticated models exist[15, 16, 17, 8, 9], but require much longer computational time to evaluate,

and so are unsuitable for databases or analysis of large datasets. The HTP has been tested on the simulated spectra of H_2, H_2O, CO_2 and O_2[11] to ensure that it gives consistent results with other models and the errors were found to be less than tenths of a percent. H_2O has a challenging lineshape to fit and the success of the HTP in doing so shows that this profile could be deployed to model molecular lineshapes in spectroscopic databases.

Using a frequency comb referenced external cavity diode laser (ECDL)[18], we recently measured the $P_e(11)$ line of the $\nu_1+\nu_3$ combination band of acetylene[19, 20] to high accuracy over a range of pressures and temperatures. This line, henceforth referred to as simply $P_e(11)$, was chosen as a strong and relatively isolated transition in a band of $^{12}C_2H_2$ located at 1.5 μm, that lies in an atmospheric window between strong interfering H_2O and CH_4 bands, enabling its use for satellite remote sensing observations. Our data clearly exhibit speed dependent and/or collisional narrowing effects, making the VP inadequate for modeling the measurements. We tested the SDVP[4, 5] and the QSDVP[21, 22, 23, 24, 25] and settled with the latter because of its more physically realistic properties[20]. With the decision of the IUPAC to standardize on the HTP, we have revisited our analysis using a new Matlab-based lineshape fitting code. We have also measured positions of several underlying hot band features that previously compromised the analysis due to their imprecisely known frequencies. The aims of this work are to : 1) use our self-broadened and N_2-broadened data sets acquired across a wide range of pressures and temperatures at a signal to noise of the order of 10^4 to further test the validity and utility of the HTP, 2) make our data the most accessible and useful by conforming to the new standard model, 3) provide a useful lineshape fitting code to the community.

2. The HTP model

A complete description of the HTP and appropriate references can be found in other papers[10, 13, 14, 11] with a FORTRAN code generating the HTP profile[13, 14]. Here, we summarize the main equations needed to code the

profile. The global form of the HTP is :

$$\mathrm{HTP}(\nu) = \frac{1}{\pi}\,\mathrm{Re}\left\{\frac{A(\nu)}{1-\left[\nu_{\mathrm{VC}}-\eta(C_0-3C_2/2)\right]A(\nu)+(\eta C_2/v_{a0}^2)B(\nu)}\right\} \tag{1}$$

with :

$$A(\nu) = \frac{\sqrt{\pi}c}{\nu_0 v_{a0}}\left[w(iZ_-)-w(iZ_+)\right] \tag{2}$$

$$B(\nu) = \frac{v_{a0}^2}{\tilde{C}_2}\left[-1+\frac{\sqrt{\pi}}{2\sqrt{Y}}(1-Z_-^2)w(iZ_-)-\frac{\sqrt{\pi}}{2\sqrt{Y}}(1-Z_+^2)w(iZ_+)\right] \tag{3}$$

Notice that A and B depend on the complex probability function :

$$w(z) = \frac{i}{\pi}\int_{-\infty}^{+\infty}\frac{e^{-t^2}}{z-t}dt = e^{-z^2}\mathrm{erfc}(-iz) \tag{4}$$

where erfc is the complex Gauss error function. $w(z)$ is also known as the Faddeyeva, Faddeeva or Kramp function and a publicly available Matlab routine[26]for this function has been used in this analysis.

The other terms in eq.1-3 are :

$$\begin{aligned} Z_\pm &= \sqrt{X+Y}\pm\sqrt{Y} \\ X &= \frac{i(\nu_0-\nu)+\tilde{C}_0}{\tilde{C}_2} \\ Y &= \left(\frac{\nu_0 v_{a0}}{2c\tilde{C}_2}\right)^2 \end{aligned} \tag{5}$$

where

$$\begin{aligned} \tilde{C}_0 &= (1-\eta)(C_0-3C_2/2)+\nu_{\mathrm{VC}} \\ \tilde{C}_2 &= (1-\eta)C_2 \end{aligned} \tag{6}$$

and

$$
\begin{aligned}
C_n &= \Gamma_n + i\Delta_n, \quad n = 0, 2 \\
v_{a0} &= \sqrt{\frac{2k_B T}{M}} = \frac{c\Gamma_D}{\sqrt{\ln(2)}\nu_0}
\end{aligned}
\tag{7}
$$

ν_0 is the center frequency of the transition; v_{a0} is the most probable speed of the active molecule of mass M at temperature T and k_B is the Boltzmann constant; c is the speed of light and Γ_D is the Doppler width.

If $\tilde{C}_2 \to 0$, which happens when $\eta \to 1$ or $C_2 \to 0$, then[13, 14]:

$$
\begin{aligned}
Z_- &= \frac{i(\nu_0 - \nu) + \tilde{C}_0}{\nu_0 v_{a0}/c} \\
A(\nu) &= \frac{\sqrt{\pi}c}{\nu_0 v_{a0}} \omega(iZ_-) \\
B(\nu) &= \frac{\sqrt{\pi}c v_{a0}}{\nu_0} \left[(1 - Z_-^2)\omega(iZ_-) + \frac{Z_-}{\sqrt{\pi}} \right]
\end{aligned}
\tag{8}
$$

These values can then be substituted into eq.1 to give the simpler, limiting cases of the HTP[10, 11] when $\eta = 0$ or $C_2 = 0$, such as the VP or the Rautian profile (RP). No other limits were considered in this paper as they did not play a role in our analysis.

In total, 8 parameters define the HTP: ν_0, v_{a0}, Γ_0, Δ_0, Γ_2, Δ_2, ν_{VC} and η. ν_0 and v_{a0}, which define the Doppler width Γ_D according to eq.7, are not adjusted. Γ_0 and Δ_0 are the usual broadening and shifting speed-independent coefficients of the relaxation rate found in the VP. However, the apparent shifting and broadening of a line depends as well on the relative collision speed between the active molecule and its collider. When averaged over all possible colliding speeds, Γ_2 and Δ_2 arise as phenomenological parameters accounting for the chosen quadratic form of the relaxation rate[1, 21] in terms of the active molecule speed v_a :

$$
\begin{aligned}
\Gamma(v_a) &= \Gamma_0 + \Gamma_2 \left[(v_a/v_{a0})^2 - 3/2) \right] \\
\Delta(v_a) &= \Delta_0 + \Delta_2 \left[(v_a/v_{a0})^2 - 3/2) \right]
\end{aligned}
\tag{9}
$$

The frequency of the velocity-changing collisions, referred to as ν_{VC}, accounts for collisional narrowing also referred to as the Dicke narrowing[27]. In the

hard collision limit and taking into account speed dependent effects, the speed-dependent velocity-changing collision frequency, or equivalently the frequency of hard collisions can be defined as eq.10 [7, 11, 27, 28]:

$$\tilde{\nu}_{VC}(v_a) = \nu_{VC} - \eta(\Gamma(v_a) + i\Delta(v_a)) \tag{10}$$

in which η represents the correlation between velocity-changing + dephasing and pure dephasing collisions of $\Gamma(v_a)$ and $\Delta(v_a)$.

In more detail, three types of collisions are assumed to occur in a molecular bath: the dephasing collisions (D), the velocity-changing collisions (VC) and collisions leading to both velocity-change and dephasing (VCD)[29]. The relaxation rate coefficients Γ and Δ and the collisional frequency ν_{CF} take the form :

$$\begin{aligned} \Gamma(v_a) &= \Gamma^D(v_a) + \Gamma^{VCD}(v_a) \\ \Delta(v_a) &= \Delta^D(v_a) + \Delta^{VCD}(v_a) \\ \nu_{\mathrm{CF}} &= \nu_{\mathrm{VC}} + \nu_{\mathrm{VCD}} \end{aligned} \tag{11}$$

In the HTP, ν_{CF} is calculated assuming no correlation between velocity changes and dephasing[11]. Therefore, $\nu_{\mathrm{VCD}} = 0$ and $\nu_{\mathrm{CF}} = \nu_{\mathrm{VC}}$.

Finally, if $\Gamma(v_a)$ and $\Delta(v_a)$ are assumed to share a common, speed-independent correlation factor η[7, 11, 27] then :

$$\begin{aligned} \eta(\Gamma(v_a) + i\Delta(v_a)) &= \Gamma^{VCD}(v_a) + i\Delta^{VCD}(v_a) \\ (1-\eta)(\Gamma(v_a) + i\Delta(v_a)) &= \Gamma^D(v_a) + i\Delta^D(v_a) \end{aligned} \tag{12}$$

As a result, both the pure dephasing and dephasing+velocity changing parts of each Γ and Δ have the same speed dependence from eq.9.

3. Effective parameters in the multispectrum fitting

Eq.1-7 fully define the HTP. Our data were recorded in transmission and the Beer-Lambert law is used to model the transmitted laser light following sample absorption :

$$HTP_T(\nu) = e^{-\mathrm{Amp}\times HTP(\nu)} \tag{13}$$

The amplitude (Amp) is a known quantity which depends on the absorption path length l_{path} (in cm) and the line strength S. In the Hitran 2012 database[30], the line strength is assumed to be proportional to the density of molecules $N = P/(k_B T)$ (in molecule.cm^{-3}) and Amp becomes:

$$\mathrm{Amp} = S_\nu^N N l_{\mathrm{path}} \tag{14}$$

Hitran 2012 reports $S_\nu^N = 1.165 \times 10^{-20}$ cm^{-1}(molecule.cm^{-2})$^{-1}$, at the reference temperature of $\mathrm{T_{ref}} = 296$ K, for the $\mathrm{P_e}(11)$ line listed at a frequency of 6529.171909 cm^{-1}[31]. In order to use the line strength at different temperatures, one has to convert S_ν^N into a temperature-dependent quantity using[32]:

$$S_\nu^N(T) = S_\nu^N(T_{\mathrm{ref}}) \frac{Q_{tot}(T_{\mathrm{ref}})}{Q_{tot}(T)} e^{-c_2 E_1 (1/T - 1/T_{\mathrm{ref}})} \left[\frac{1 - e^{-c_2 \nu / T}}{1 - e^{-c_2 \nu / T_{\mathrm{ref}}}} \right] \tag{15}$$

where $c_2 = hc/k_B$ is in cm.K with h the Planck constant and c the speed of light. E_1 is the energy, in cm^{-1}, of the lower energy level. Finally, $Q_{tot}(T)$ is the total internal partition sum of the active molecule, at temperature T. In our case, $E_1 = 155.289$ cm^{-1} is found in Hitran 2012 and the partition function is given as a polynomial expansion in the temperature[33]:

$$Q_{tot}(T) = -8.3088 + 1.4484T - 2.5946 \times 10^{-3} T^2 + 8.4612 \times 10^{-6} T^3 \tag{16}$$

Finally, experimental baseline drifts are modeled with a degree 2 polynomial. The final expression used to model the transmitted beam after absorption is:

$$HTP_T(\nu) = e^{-\mathrm{Amp}\times HTP(\nu)} (b_0 + (\nu - \nu_0) \times b_1 + (\nu - \nu_0)^2 \times b_2) \tag{17}$$

A code written in Matlab to generate and fit a HTP, as well as the derivatives of the HTP explicitly written are given as a supplementary material. Note that the routine needs the Faddeyeva function[26] to be placed in the same folder.

Eq.17 is valid for one line. However, it is not suitable for modeling a single experimental transition measurement with all parameters floating because the

resulting high number of correlated parameters makes the fit unstable. We used a multispectrum fitting approach[34] and used constraints on the pressure and temperature-dependent parameters to reduce the number of free parameters. While η is assumed independent of both the pressure and temperature[11], all the other 5 fitted HTP parameters Γ_0, Γ_2, Δ_0, Δ_2 and ν_{VC} are linear in the pressure. A power law temperature dependence, as used in the Hitran[30] representation, was found to be suitable for all these parameters except Δ_2, which was freely adjusted at each temperature. Therefore, a typical pressure and temperature dependent parameter X takes the form:

$$\begin{aligned} X(T,P) &= X(T_{\mathrm{ref}} = 296, P_{\mathrm{ref}} = 1 \text{ atm}) \left(\frac{296}{T}\right)^{n_X} \left(\frac{P}{P_{\mathrm{ref}}}\right) \\ &= X_{\mathrm{ref}} \left(\frac{296}{T}\right)^{n_X} P \end{aligned} \tag{18}$$

assuming the pressure is reported in atm. For each such pressure and temperature dependent parameter $X(T,P)$, 2 pressure and temperature independent parameters are reported: X_{ref} and n_X.

The quadratic baseline was floating for each measured spectrum data file, and the possibility that a line was spread over several files was also allowed. This happened particularly at higher pressures and temperatures where the broadening of the lines was such that the spectrometer could not entirely scan it in one pass. Since then, the spectrometer has been modified to scan much longer regions and an example is given in the top trace in fig.1.

Since we can define a temperature and pressure dependent expression of the amplitude which depends on the constant $S_\nu^N(T_{\mathrm{ref}})$, we used our self-broadened data set to estimate this quantity in the multispectrum fit and compare it with the Hitran 2012[30] value. The acetylene concentration in the N_2-broadened data set was on the order of only 1%, and subject to larger relative error, which did not permit the use of only one floating parameter, $S_\nu^N(T_{\mathrm{ref}})$, to determine the amplitude of the transitions in the same scheme. Instead, we allowed the parameter Amp to float for each line in the N_2-broadened data, to account for any small acetylene concentration measurement error. The cell length variation

l_{path} with the temperature is negligible[20] and has not been taken into account.

The HTP parameters also had to be modified to account for a mixture in our N_2-broadened data set. If we denote by χ_i the mole fraction of species i in the mixture, then we have[11] :

$$\begin{aligned} \nu_{\text{VC}} &= \sum_i \chi_i \nu_{\text{VC}}^i \\ C_n &= \sum_i \chi_i C_n^i \\ \eta C_n &= \sum_i \chi_i \eta^i C_n^i \end{aligned} \tag{19}$$

Finally, for a more balanced treatment of the contributions from individual lines to the total error to be minimized in the multispectum analysis, each line has been scaled to a common transmission at line center, arbitrarily chosen to be 0.5, following the approach taken by Ngo, et al.[11]. This was achieved by retrieving the minimum transmission value (min) and applying the scaling:

$$\begin{aligned} \text{scaled line} &= 1 - (1 - \text{original line}) \times \frac{0.5}{1 - \text{min}} \\ &= \frac{0.5 - \text{min}}{1 - \text{min}} + \frac{0.5}{1 - \text{min}} \times \text{original line} \\ &= \text{offset} + \alpha \times \text{original line} \end{aligned} \tag{20}$$

The corresponding synthetic line in the fitting routine was scaled with the same values of α and offset prior to computing the partial contribution to the residual from that line. This scaling has the effect of weighting the individual lines so as to minimize the combined relative errors of all lines in the multi-spectrum fit. This increases the weight of weak lines relative to strong lines compared to an unscaled multispectral analysis. In addition, the fitting routine made 2 passes through the data. The first one included all the data points while the second excluded data points for which their residuals were more that 4 standard deviations away.

4. Hot bands near $P_e(11)$

As measurement techniques become more and more sensitive, spectra reveal features that were previously ignored. Hot bands in the region of interest are 500-5000 times weaker than $P_e(11)$ but are clearly visible in fig.1. This spectrum has been recorded after substantial improvements of the spectrometer to reduce noise and to scan much longer spectral regions without having to reposition the spectrometer in frequency space. Only a handful of such scans were recorded and they have not been included in the overall multispectrum fitting because baseline drifts over the long scans were difficult to account for using the quadratic form described above.

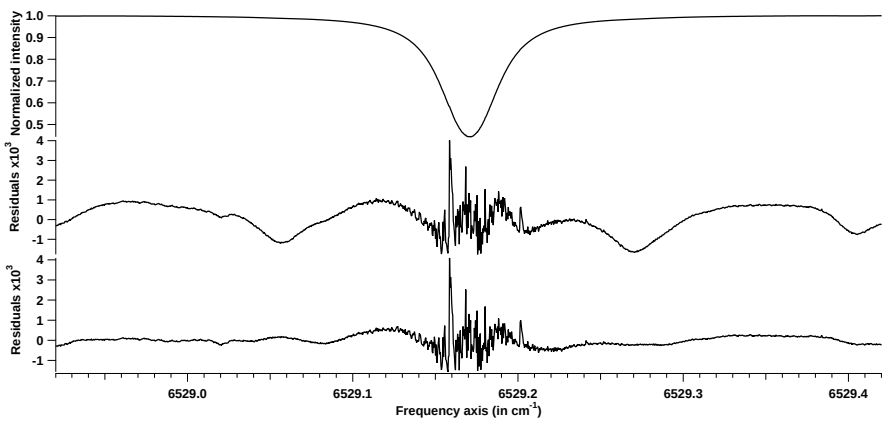

Figure 1: The top panel shows a low noise spectrum of $P_e(11)$. The medium panel shows the observed-calculated residuals after the line was fit with the HTP. The hot band lines clearly appear visible. The bottom panel shows the fit after the hot band transitions have been accounted for. A complete line list of the hot band transitions modeled in this work is given in tables 1 and 2.

In order to model the $P_e(11)$ lineshape accurately, five accessible nearby hot band absorptions have been newly measured in the sub-Doppler limit using the same spectrometer to record their rest frequencies[35]. The updated hot band rest frequencies and their characteristics are given in tables 1 and 2, the parameter definition echoing eq.18. The lines are labeled according to Hitran 2012[30] where $T_{ref} = 296K$ and in which the upper and lower states are denoted by at

least 5 numbers referring to the vibrational quantum numbers ν_1, ν_2, ν_3, ν_4, ν_5. The 6th number indicates $l = |l_4 + l_5|$[36] where l_4 and l_5 refer to the bending vibrational angular momenta[37]. If relevant, the 7th number indicates the rank of the level, 1 being the highest level in energy[36]. The characteristics of the hot band transitions were taken from Hitran 2012[30] although the Q branch 101101u-000101g is missing from the database. The frequencies of these missing Q lines 101101u-000101g were determined by diagonalizing a Hamiltonian built on the polyad scheme[38], while their line strengths were estimated by using the line strengths of the P and R lines of the same vibronic transition scaled by the proper Höln-London factors[39, 40].

The parameters defined in air were used for the N_2 mixture data[30]. Note that not all the needed parameters were available. When missing, the parameters for $P_e(11)$ were assumed.

Table 1: Characteristics of the hot band lines included in the $P_e(11)$ lineshape modeling.

Line	transition label [c]	rest frequency cm^{-1}	$S_\nu^N(T_{ref})$ $cm^{-1}.(mol.cm^{-2})^{-1}$	E_1 [d] cm^{-1}
$Q_e(11)$ [b]	101101u-000101g	6528.8572	$8.40.10^{-23}$	766.8079
$P_f(15)$	200101g-000011u	6528.897133 [a]	$2.070.10^{-23}$	1012.5316
$P_e(25)$	1102112u-000101g	6528.9311	$2.481.10^{-24}$	1374.9612
$P_e(15)$	200101g-000011u	6528.9311	$7.396.10^{-24}$	1011.4062
$Q_e(10)$ [b]	101101u-000101g	6529.0156	$3.48.10^{-24}$	740.9595
$R_f(6)$	101022u-000022g	6529.057503 [a]	$7.465.10^{-24}$	1507.8826
$Q_f(6)$ [b]	101101u-000101g	6529.0577	$2.49.10^{-23}$	661.2741
$R_e(6)$	101022u-000022g	6529.0846	$2.488.10^{-24}$	1507.8868
$R_e(9)$	101110+g-000110+u	6529.1363	$5.362.10^{-24}$	1434.2887
$Q_e(9)$ [b]	101101u-000101g	6529.1602	$1.29.10^{-23}$	717.4596
$R_e(11)$	101200+u-000200+g	6529.199830 [a]	$2.250.10^{-23}$	1386.3099
$R_f(10)$	101112g-000112u	6529.2514	$5.847.10^{-24}$	1472.5646
$R_e(10)$	101112g-000112u	6529.270875 [a]	$1.754.10^{-23}$	1472.5850
$Q_f(5)$ [b]	101101u-000101g	6529.2724	$1.05.10^{-23}$	647.1089
$Q_e(8)$ [b]	101101u-000101g	6529.2900	$5.37.10^{-24}$	696.3086
$Q_e(7)$ [b]	101101u-000101g	6529.4054	$1.98.10^{-23}$	677.5068
$Q_f(4)$ [b]	101101u-000101g	6529.451001 [a]	$4.10.10^{-23}$	635.3042

[a] rest frequencies determined by sub-Doppler spectroscopy in our laboratory[35].

[b] Lines not listed in Hitran 2012[30]. Their rest frequencies have been calculated using a polyad based Hamiltonian[38].

[c] upper state - lower state, see text for more details.

[d] lower state energy.

Table 2: Lineshape parameters used to model the hot band transitions included in the $P_e(11)$ lineshape modeling.

Line	transition label[b]	Γ_0^{air} $cm^{-1}.atm^{-1}$	n_Γ^{air}	Γ_0^{self} $cm^{-1}.atm^{-1}$
$Q_e(11)^a$	101101u-000101g	0.0800	0.75	0.150
$P_f(15)$	200101g-000011u	0.0756	0.75	0.138
$P_e(25)$	1102112u-000101g	0.0597	0.75	0.110
$P_e(15)$	200101g-000011u	0.0756	0.75	0.138
$Q_e(10)^a$	101101u-000101g	0.0800	0.75	0.150
$R_f(6)$	101022u-000022g	0.0852	0.75	0.166
$Q_f(6)^a$	101101u-000101g	0.0800	0.75	0.150
$R_e(6)$	101022u-000022g	0.0852	0.75	0.166
$R_e(9)$	101110+g-000110+u	0.0808	0.75	0.154
$Q_e(9)^a$	101101u-000101g	0.0800	0.75	0.150
$R_e(11)$	101200+u-000200+g	0.0787	0.75	0.147
$R_f(10)$	101112g-000112u	0.0796	0.75	0.150
$R_e(10)$	101112g-000112u	0.0796	0.75	0.150
$Q_f(5)^a$	101101u-000101g	0.0800	0.75	0.150
$Q_e(8)^a$	101101u-000101g	0.0800	0.75	0.150
$Q_f(7)^a$	101101u-000101g	0.0800	0.75	0.150
$Q_e(4)^a$	101101u-000101g	0.0800	0.75	0.150

[a] Lines not listed in Hitran 2012[30].

[b] Upper state - lower state, see text for more details.

Correctly modeling the hot band lines is critical to extract precise parameters for the main feature. For example, $R_e(11)$ of the $2\nu_4$ hot band is listed at 6529.196200 cm^{-1} in Hitran 2012[30], but turns out to be 100 MHz away at 6529.199830 cm^{-1} when remeasured. Moreover, it is a line which is very close to the center of our line of interest $P_e(11)$. Fig.2 shows the temperature dependence of the line strength for selected hot band lines in the vicinity of $P_e(11)$, normalized to the line strength of $P_e(11)$. A few hot band lines have relative line strengths that begin to become appreciable compared to the experimental sensitivity at a temperature of about 240 K, due to the higher energy of the lower level involved compared to that of $P_e(11)$. $R_e(11)$ of $2\nu_4$ in particular reaches values well above our experimental signal to noise ratio, determined to be below 1 part in 10^4.

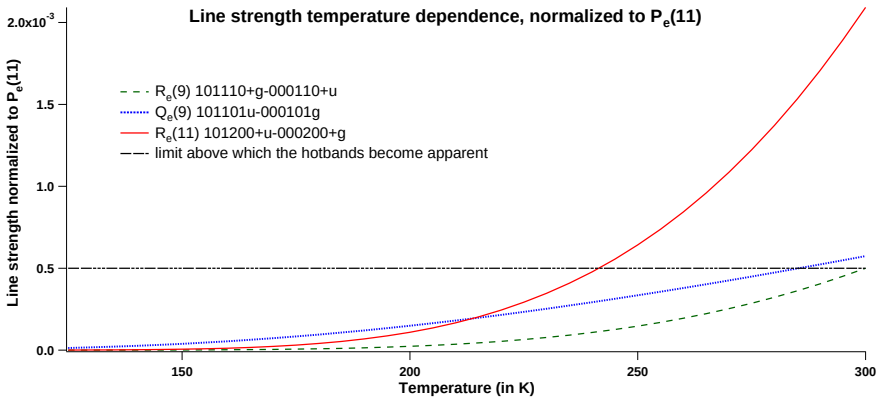

Figure 2: Line strengths of the hot band transitions in the vicinity of $P_e(11)$, normalized to the line strength of $P_e(11)$. Only the closest hot band lines are represented, labeled according to table 1 and 2.

5. Results

Before analyzing the experimental data, we compared our QSDVP^t[20, 25] (t denoting that the function was calculated in the time domain, as opposed to using the QSDVP form of the HTP) and the HTP on a synthetic data set using the multispectrum fitting approach, by setting ν_{VC} and η to 0. The QSDVP^t was calculated by taking the numerical Fourier transform of an analytic time-domain correlation function. The maximum time considered and time interval used to evaluate the correlation function were critical to ensure both reliable and fast calculations. With the settings previously used[20], the two models differ at the 10^{-6} level, much lower than our sensitivity and therefore yield the same results, well within experimental limits. By taking larger maximum times and smaller time intervals, we can reduce this difference at the cost of a higher computation time when computing the QSDVP^t in the time domain.

The self-broadened data set contains 64 lines acquired at temperatures ranging from 150 K to 296 K and pressures from 4 to 355 Torr. The N_2-broadened data set contains 61 lines acquired at temperatures ranging from 125 K to 296 K and pressures from 5 Torr to 1 atmosphere. The final results for both analyses are presented in table 3 and table 4, respectively.

Table 3: Lineshape constants for the self-broadened data set.

Parameter[a]		HTP	QSDVP	QSDVP[t] [20]
n_{Γ_0}		0.6917(23)	0.6866(30)	0.69(1)
Γ_0		0.15383(16)	0.15472(20)	0.1548(11)
n_{Δ_0}		0.0829(87)	0.0816(98)	0.05(1)
Δ_0		-0.008058(38)	-0.008013(41)	-0.00817(5)
n_{Γ_2}		0.832(24)	0.669(19)	0.66(4)
Γ_2		0.01984(28)	0.02119(18)	0.0214(6)
$n_{\nu_{\mathrm{VC}}}$		0.28(22)	0	0
ν_{VC}		0.0258(44)	0	0
η		0.124(30)	0	0
$S_\nu^N(T_{\mathrm{ref}})\ \times 10^{20}$ [f]		1.2001(50)	1.2014(50)	1.165[e]
Δ_2[b]	150.383(20)	-0.00218(12)	-0.001651(50)	-0.00166(2)
	155.373(30)	-0.00199(11)	-0.001489(54)	-0.00156(4)
	160.343(50)	-0.001873(98)	-0.001477(47)	-0.00154(4)
	165.373(12)	-0.001716(99)	-0.001410(59)	-0.00148(5)
	175.319(16)	-0.001733(87)	-0.001359(60)	-0.00139(3)
	200.298(49)	-0.001536(86)	-0.001232(55)	-0.00134(6)
	240.135(25)	-0.00170(10)	-0.001303(73)	-0.00144(5)
	295.715(19)	-0.00180(13)	-0.001324(98)	-0.00169(6)
rmse[c]		1.7×10^{-4}	1.7×10^{-4}	0.9×10^{-4} [d]

[a] All parameters in $\mathrm{cm}^{-1}.\mathrm{atm}^{-1}$, except for the exponents and η which are dimensionless.

[b] Calculated for each temperature data set, the average temperature being given in the adjacent column in Kelvin.

[c] Weighted rmse of the fit.

[d] rmse of fit to unscaled data, see text for details.

[e] fixed values from [30]

[f] in units of $\mathrm{cm}^{-1}.(\mathrm{mol.cm}^{-2})^{-1}$

Numbers in parentheses are 1σ uncertainties in the last digits.

From such a multispectrum analysis, the statistical error in the parameters can be misleading in that they will be lower than one would expect due to the the neglect of systematic measurement errors. For example, table 5 shows results from fitting a synthetic data set to which noise similar, discussed in more detail below, to the noise observed in the experiment was added. The error bounds, calculated on the assumption that the noise is purely Gaussian, are clearly too restrictive. In order to give a more realistic error bound on our reported lineshape parameters, we adopted a Monte-Carlo method similar to that described previously[20]. Multiple synthetic multispectrum data sets,

Table 4: Lineshape constants for the N_2-broadened data set.

Parameter[a]		HTP	QSDVP	QSDVP[t] [20]
n_{Γ_0}		0.7373(29)	0.7378(25)	0.738(9)
Γ_0		0.08834(10)	0.08937(10)	0.0894(5)
n_{Δ_0}		0.5719(32)	0.5820(32)	0.583(6)
Δ_0		-0.009392(15)	-0.009288(16)	-0.00935(3)
n_{Γ_2}		0.207(41)	0.473(14)	0.46(4)
Γ_2		0.01426(20)	0.013848(95)	0.0138(2)
$n_{\nu_{VC}}$		1.34(11)	0	0
ν_{VC}		0.0107(13)	0	0
η		0.129(16)	0	0
Δ_2[b]	125.300(20)	-0.00302(12)	-0.002076(36)	-0.00231(7)
	140.117(44)	-0.00218(10)	-0.001371(34)	-0.00126(7)
	160.128(33)	-0.001962(87)	-0.001297(26)	-0.00138(7)
	175.281(96)	-0.001203(82)	-0.000515(41)	-0.00074(7)
	200.145(71)	-0.001109(69)	-0.000667(35)	-0.00063(5)
	240.080(20)	-0.001008(54)	-0.000588(24)	-0.00041(6)
	295.851(19)	-0.001123(48)	-0.000735(23)	-0.00060(5)
rmse[c]		2.4×10^{-4}	2.5×10^{-4}	0.9×10^{-4} [d]

[a] All parameters in $cm^{-1}.atm^{-1}$, except for the exponents and η which are dimensionless.

[b] Calculated for each temperature data set, the average temperature being given in the adjacent column in Kelvin.

[c] Weighted rmse of the fit.

[d] rmse of fit to unscaled data, see text for details.

Numbers in parentheses are 1σ uncertainties in the last digits.

similar to the self- and N_2-broadened data sets, were generated such that each experimentally measured quantity was varied over a range defined by a Gaussian distribution centered at their measured values and in terms of the estimated standard deviation of the measurement error.

Pressure measurement errors were accounted for by assuming a systematic error equivalent to a standard deviation of 10 mT for each synthesized data set. Within each data set, pressure measurement noise of 0.3% was assumed for each measured line. For the frequency axis, a 50 kHz standard deviation was assumed except for hot band lines whose frequencies have not been measured, where 0.002 cm^{-1} was assumed. Lineshape parameters for the hot band lines were assumed to have errors of 10%. The data were recorded by taking the ratio of a reference channel and the absorbed channel, subject to random noise

as well, on the order of 10^{-4} and this was added in the synthetic model. Finally, the baseline drift could not, in most cases, be entirely modeled by a second order polynomial and so a cubic noise term was added with a standard deviation set to reproduce the similar baseline drifts we observed.

500 data sets were generated and then fit, for each of the four scenarios: self- and N_2-broadened sets and each of the HTP and QSDVP lineshape functions. The final parameter errors were defined as the standard deviation of each lineshape parameter across the 500 fits of the synthetic data set and are reported in tables 3 and 4. Note that the reported root mean square error (rmse) values for the present analysis that used scaled data and are therefoe not directly comparable to the previous unscaled fits to the same data[20] shown in the final column of tables 3 and 4.

6. Discussion

The velocity changing collision parameter ν_{VC} is related to the mass diffusion coefficient through $\nu_{\mathrm{VC}} = k_B T/(2\pi M c D)$[11] where M is the mass of the active molecule, C_2H_2, and D is the mass diffusion coefficient which can be calculated solely based on the molecular gas properties[41]. The HTP allows fits to both Γ_2 and ν_{VC} simultaneously, which was not possible previously with the QSDVP^t[20] due to the high correlation between the parameters making the fit unstable. One expects ν_{VC} to take the form of a power law in the temperature (cf eq.18) with an exponent close to 1 because D is expected to vary approximately as T^2[11, 41]. Our exponents for the self- and N_2-broadened data sets were found to be 0.28 and 1.36 respectively, quite far from 1. However, there are substantial correlations between the exponents of Γ_2 and ν_{VC} still remaining and in order to better measure the impact of ν_{VC} we used the RP form of the HTP to extract the pressure and temperature independent parameters defining ν_{VC}. The exponents came out closer to 1 at 0.63 and 0.80 respectively for the self- and N_2-broadened data sets, with values across the temperatures matching relatively well as shown in table 6. However, we did not keep the Rautian form of the HTP because the

Table 5: Fit of a synthetic data set subject to similar noise found in the self- and N_2-broadened data sets.

Parameter[a]		HTP	True values
n_{Γ_0}		0.67715(31)	0.68
Γ_0		0.149542(25)	0.15
n_{Δ_0}		0.0474(46)	0.053
Δ_0		-0.008028(15)	-0.008
n_{Γ_2}		0.476(12)	0.6
Γ_2		0.01969(13)	0.02
$n_{\nu_{\mathrm{VC}}}$		0.790(15)	0.7
ν_{VC}		0.0329(12)	0.03
η		0.2130(79)	0.2
$S_\nu^N(T_{\mathrm{ref}})\ \times 10^{20}$ [d]		1.16185(10)	1.165
Δ_2[b]	150	-0.002594(74)	-0.0024
	155	-0.002590(78)	-0.0024
	160	-0.002548(67)	-0.0024
	165	-0.002559(100)	-0.0024
	175	-0.002709(85)	-0.0024
	200	-0.002628(62)	-0.0024
	240	-0.002558(54)	-0.0024
	295	-0.002552(68)	-0.0024
rmse[c]		1.9×10^{-4}	N/A

[a] All parameters in $\mathrm{cm}^{-1}.\mathrm{atm}^{-1}$, except for the exponents and η which are dimensionless.
[b] Calculated for each temperature data set, the average temperature being given in the adjacent column in Kelvin.
[c] Weighted rmse of the fit.
[d] in units of $\mathrm{cm}^{-1}.(\mathrm{mol.cm}^{-2})^{-1}$
Numbers in parentheses are 1σ uncertainties in the last digits.

rmse of the fit is 2 times worse than for the full HTP or QSDVP form.

The difference in the quality of the fit between the QSDVP and the Rautian form of the HTP suggests that the collisional processes happening in our cell are mostly due to speed dependent and dephasing effects. This conclusion is further supported by the low correlation parameter η of the full HTP form, suggesting that the collisions are mostly purely dephasing.

The speed dependent parameter Δ_2 did not follow a power law distribution in the temperature. The downward trend past 200 K observed in our previous work[20] could be reproduced by simulating multispectra datasets in which the hot band lines were not accounted for. This is consistent with fig.2

Table 6: Velocity changing rate coefficients for the HTP and the RP at different temperatures and a pressure of 1 atm.

Temperature (in K)	Self-broadened			N_2-broadened		
	HTP	RP	Theory[a]	HTP	RP	Theory[a]
296	0.026	0.049	0.040	0.011	0.022	0.031
240	0.027	0.055	0.048	0.015	0.026	0.037
200	0.029	0.062	0.058	0.019	0.031	0.044
175	0.030	0.068	0.066	0.023	0.034	0.050
165	0.030	0.070	0.070	0.025	0.036	0.052
160	0.031	0.072	0.072	0.026	0.036	0.054
155	0.031	0.073	0.074	0.027	0.037	0.056
150	0.031	0.075	0.077	0.028	0.038	0.057
125	0.033	0.084	0.092	0.036	0.044	0.069

[a] [41].

All numbers, except the temperatures, are in cm^{-1}.

which shows that the hot band lines can have intensities greater that our noise level at temperatures above 240 K. The present analysis shows a trend in the temperature-dependent Δ_2 term which reaches a constant value, suggesting that the hot band transitions have been more properly accounted for. However, small pressure measurement errors and baseline drifts are still uncharacterized sources of noise that primarily affect the second order parameters in the lineshape modeling.

Finally, for both our self- and N_2-broadened data sets, our experimental sensitivity is not high enough to take advantage of the full form of the HTP as it offers only a marginal improvement on the overall rmse calculated while introducing correlations between the second order parameters Γ_2, Δ_2 and ν_{VC}. As such, the parameters could lose part of their physical meaning and we recommend to use parameters of the QSDVP form reported in tables 3 and 4 to describe the $P_e(11)$ of the $\nu_1 + \nu_3$ combination band.

7. Conclusion

We have presented a new analysis of $P_e(11)$ of the $\nu_1 + \nu_3$ combination band of acetylene using the new HTP lineshape model, which successfully fit our data set with measurements across multiple temperatures and pressures. Improve-

ments to our spectrometer have allowed us to observe multiple underlying hot band transitions, which have been assigned and accounted for and, for some, newly frequency-measured at the sub-Doppler level. The measurements lead to a refined estimate of the line strength for $P_e(11)$ and determined that the QSDVP form of the HTP, which yields same quality results as the HTP but with fewer parameters, is the most suitable for these data.

8. Acknowledgments

We thank Prof. Robert Gamache (University of Massachussetts) for discussions that motivated this work. We are also grateful to Prof. David Perry (University of Akron) who provided us with the results of the global polyad Hamiltonian for acetylene and to Prof. Hiroyuki Sasada (Keio University) who helped us identify several of the hot band lines in our spectra. Work at Brookhaven National Laboratory was carried out under Contract No. DE-SC0012704 with the U.S. Department of Energy, Office of Science, and supported by its Division of Chemical Sciences, Geosciences and Biosciences within the Office of Basic Energy Sciences.

9. References

[1] F. Rohart, A. Ellendt, F. Kaghat, H. Mäder, Self and polar foreign gas line broadening and frequency shifting of CH_3F: effect of the speed dependence observed by millimeter wave coherent transients, J. Mol. Spectrosc. 185 (1997) 222–233.

[2] R. Dicke, The effect of collisions upon the Doppler width of spectral lines, Phys. Rev. 89 (1953) 472–473.

[3] J. M. Hartmann, C. Boulet, D. Robert, Collisional effects on molecular spectra: Laboratory experiments and models, consequences for applications, Elsevier: Amsterdam, 2008.

[4] P. R. Berman, Speed-dependent collisional width and shift parameters in spectral profiles, J. Quant. Spectrosc. Radiat. Transfer 12 (1972) 1331–1342.

[5] J. Ward, J. Cooper, E. W. Smith, Correlation effects in the theory of combined Doppler and pressure broadening –I. Classical theory, J. Quant. Spectrosc. Radiat. Transfer 14 (1974) 555–590.

[6] L. Galatry, Simultaneous effect of Doppler and foreign gas broadening on spectral lines, Phys. Rev. 122 (1961) 1218–1223.

[7] S. G. Rautian, I. I. Sobel'man, The effect of collisions on the Doppler broadening of spectral lines, Sov. Phys. Usp. 9 (1967) 701–716.

[8] H. Tran, F. Thibault, J.-M. Hartmann, Collision-induced velocity changes from molecular dynamic simulations in H_2-Ar: a test of the Keilson-Storer model and of line-broadening/shifting calculations for the Q(1) Raman line, J. Quant. Spectrosc. Radiat. Transfer 112 (2011) 1035–1042.

[9] H. Tran, J. M. Hartmann, F. Chaussard, M. Gupta, An isolated line-shape model based on the Keilson-Storer function for velocity changes. II. Molecular dynamics simulations and the Q(1) lines for pure H_2, J. Chem. Phys. 131 (2009) 154303.

[10] J. Tennyson, P. F. Bernath, A. Campargue, A. G. Császár, L. Daumont, R. R. Gamache, J. T. Hodges, D. Lisak, O. V. Naumenko, L. S. Rothman, H. Tran, N. F. Zobov, J. Buldyreva, C. D. Boone, M. D. D. Vizia, L. Gianfrani, J.-M. Hartmann, R. McPheat, D. Weidmann, J. Murray, N. H. Ngo, O. L. Polyansky, Recommended isolated-line profile for representing high-resolution spectroscopic transitions (IUPAC Technical Report), Pure Appl. Chem. 86 (12) (2014) 1931–1943.

[11] N. H. Ngo, D. Lisak, H. Tran, J.-M. Hartmann, An isolated line-shape model to go beyond the Voigt profile in spectroscopic databases and ra-

diative transfer codes, J. Quant. Spectrosc. Radiat. Transfer 129 (2013) 89–100.

[12] D. Lisak, N. H. Ngo, H. Tran, J.-M. Hartmann, Spectral line-shape model to replace the Voigt profile in spectroscopic databases, 13th HITRAN/Atmospheric Spectroscopy Applications Conference-doi:10.5281/zenodo.11153.

[13] H. Tran, N. H. Ngo, J. M. Hartmann, Efficient computation of some speed-dependent isolated line profiles, J. Quant. Spectrosc. Radiat. Transfer 129 (2013) 199–203.

[14] H. Tran, N. H. Ngo, J. M. Hartmann, Erratum to Efficient computation of some speed-dependent isolated line profiles [J. Quant. Spectrosc. Radiat. Transfer 129 (2013) 199-203], J. Quant. Spectrosc. Radiat. Transfer 134 (2014) 104.

[15] J. M. Hartmann, H. Tran, N. H. Ngo, X. Landsheere, P. Chelin, Y. Lu, A. W. Liu, S. M. Hu, L. Gianfrani, G. Casa, A. Castrillo, M. Lepère, Q. Delière, M. Dhyne, L. Fissiaux, Ab initio calculations of the spectral shapes of CO_2 isolated lines including non-Voigt effects and comparisons with experiments, Phys. Rev. A 87 (013403) 2013.

[16] J. M. Hartmann, V. Sironneau, C. Boulet, T. Svensson, J. T. Hodges, C. T. Xu, Collisional broadening and spectral shapes of absorption lines of free and nanopore-confined O_2 gas, Phys. Rev. A 87 (2013) 032510.

[17] N. H. Ngo, H. Tran, R. R. Gamache, D. Bermejo, J. L. Domenech, Influence of velocity effects on the shape of N_2 (and air) broadened H_2O lines revisited with classical molecular dynamics simulations, J. Chem. Phys. 137 (2012) 064302.

[18] C. P. McRaven, M. J. Cich, G. V. Lopez, T. J. Sears, D. Hurtmans, A. W. Mantz, Frequency comb-referenced measurements of self- and nitrogen-

broadening in the $\nu_1 + \nu_3$ band of acetylene, J. Mol. Spectrosc. 266 (1) (2011) 43–51.

[19] M. J. Cich, C. P. McRaven, G. V. Lopez, T. J. Sears, D. Hurtmans, A. W. Mantz, Temperature-dependent pressure broadened line shape measurements in the $\nu_1 + \nu_3$ band of acetylene using a diode laser referenced to a frequency comb, Appl. Phys. B: Lasers Opt. 109(3) (2012) 373–384.

[20] M. J. Cich, D. Forthomme, C. P. McRaven, G. V. . Lopez, G. E. Hall, T. J. Sears, A. W. Mantz, Temperature-dependent, nitrogen-perturbed line shape measurements in the $\nu_1 + \nu_3$ band of acetylene using a diode laser referenced to a frequency comb, J. Phys. Chem. A 117 (2013) 13908–13918.

[21] F. Rohart, H. Mäder, H. W. Nicolaisen, Speed dependence of rotational relaxation induced by foreign gas collisions: studies on CH_3F by millimeter wave coherent transients, J. Chem. Phys. 101 (1994) 6475–6486.

[22] R. Ciuryło, J. Szudy, Speed-dependent pressure broadening and shift in the soft collision approximation, J. Quant. Spectrosc. Radiat. Transfer 57 (1997) 411–423.

[23] D. Priem, F. Rohart, J. M. Colmont, G. Wlodarczak, J. P. Bouanich, Lineshape study of the $J = 3 \leftarrow 2$ rotational transition of CO perturbed by N_2 and O_2, J. Mol. Struct. 517 (2000) 435–454.

[24] J. F. DEu, B. Lemoine, F. Rohart, Infrared HCN lineshapes as a test of Galatry and speed-dependent Voigt profiles, J. Mol. Spectrosc. 212 (2002) 96–110.

[25] D. Forthomme, C. P. McRaven, T. J. Sears, G. E. Hall, Argon-induced pressure broadening, shifting, and narrowing in the CN $A^2\Pi$-$X^2\Sigma^+$ (1-0) band, J. Phys. Chem. A 117 (2013) 11837–11846.

[26] M. R. Zaghloul, A. N. Ali, Algorithm 916: computing the Faddeyeva and Voigt functions, ACM Trans. Math. Softw. 38,2, article 15.

doi:10.1145/2049673.2049679.
URL http://doi.acm.org/10.1145/2049673.2049679

[27] A. S. Pine, Asymmetries and correlations in speed-dependent Dicke-narrowed line shapes of argon-broadened HF, J. Quant. Spectrosc. Radiat. Transfer 62 (1999) 397–423.

[28] R. Ciuryło, A. S. Pine, J. Szudy, A generalized speed-dependent line profile combining soft and hard partially correlated Dicke-narrowing collisions, J. Quant. Spectrosc. Radiat. Transfer 68 (2001) 257–271.

[29] P. Joubert, J. Bonamy, D. Robert, J. L. Domenech, D. Bermejo, A partially correlated strong collision model for velocity- and state-changing collisions application to Ar-broadened HF rovibrational line shape, J. Quant. Spectrosc. Radiat. Transfer 61 (1999) 519–531.

[30] L. S. Rothman, I. E. Gordon, Y. Babikov, A. Barbe, D. C. Benner, P. F. Bernath, M. Birk, L. Bizzocchi, V. Boudon, L. R. B. et al., The HITRAN2012 molecular spectroscopic database, J. Quant. Spectrosc. Radiat. Transfer 130 (2013) 4–50.

[31] A. A. Madej, A. J. Alcock, A. Czajkowski, J. E. Bernard, S. Chepurov, Accurate absolute reference frequencies from 1511 to 1545 nm of the $\nu_1 + \nu_3$ band of $^{12}C_2H_2$ determined with laser frequency comb interval measurements, J. Opt. Soc. Am. B 23 (2006) 2200–2208.

[32] M. Šimečková, D. Jacquemart, L. S. Rothman, R. R. Gamache, A. Goldman, Einstein A-coefficients and statistical weights for molecular absorption transitions in the HITRAN database, J. Quant. Spectrosc. Radiat. Transfer 98 (2006) 130–155.

[33] R. R. Gamache, S. Kennedy, R. Hawkins, L. S. Rothman, Total internal partition sums for molecules in the terrestrial atmosphere, J. Mol. Struct. 517-518 (2000) 407–425.

[34] D. C. Benner, C. P. Rinsland, V. M. Devi, M. A. H. Smith, D. Atkins, A multispectrum nonlinear least squares fitting technique, J. Quant. Spectrosc. Radiat. Transfer 53 (1995) 705–721.

[35] S. Twagirayezu, M. J. Cich, T. J. Sears, C. P. McRaven, G. E. Hall, Frequency comb-referenced spectroscopy of ν_4 and ν_5 hot bands in the $\nu_1 + \nu_3$ combination band of C_2H_2 (TBP).

[36] D. Jacquemart, J. Y. Mandin, V. Dana, C. Claveau, J. V. Auwera, M. Herman, L. S. Rothman, L. Régalia-Jarlot, A. Barbe, The IR acetylene spectrum in HITRAN: update and new results, J. Quant. Spectrosc. Radiat. Transfer 82 (2003) 363–382.

[37] M. Herman, A. Campargue, M. I. E. Idrissi, J. V. Auwera, Vibrational Spectroscopic Database on Acetylene, $\tilde{X}^1\Sigma_g^+$ ($^{12}C_2H_2$, $^{12}C_2D_2$ and $^{13}C_2H_2$), J. Phys. Chem. Ref. Data 32 (2003) 921–1361.

[38] M. Herman, D. S. Perry, Molecular spectroscopy and dynamics: a polyad-based perspective, Phys. Chem. Chem. Phys. 15 (2013) 9970–9993.

[39] O. M. Lyulin, D. Jacquemart, N. Lacome, V. I. Perevalov, J. Y. Mandin, Line parameters of acetylene in the 1.9 and 1.7 μm spectral regions, J. Quant. Spectrosc. Radiat. Transfer 109 (2008) 1856–1874.

[40] R. El Hachtouki, J. Vander Auwera, Absolute line intensities in acetylene: the 1.5 μm region, J. Mol. Spectrosc. 216 (2002) 355–362.

[41] J. O. Hirschfelder, C. F. Curtiss, R. B. Bird, Molecular Theory of Gases and Liquids, Vol. 26, Wiley: New York, 1954.

1. Supplemental information: derivatives of the HTP model

We present here analytic derivatives of the HTP function with respect to its various parameters for use in iterative nonlinear parameter fitting routines, such as the one implemented in the supporting information. Although we did not float the Doppler width Γ_D nor the rest frequency ν_0 and therefore did not calculate these derivatives in the code, we included them in the subsequent derivations, for completeness. Note that the Doppler width depends on ν_0 and the temperature T. ν_0 can be floated separately and the most probable speed v_{a0} is the only parameter which depends on T. Therefore, we will limit ourselves to the calculation of the derivatives with respect to ν_0 and v_{a0}, from which the Doppler width can then be deduced.

Let us start with a few simple derivatives that we will refer to later on, starting by the derivative of the Faddeyeva function. We adopt the convention to label the derivatives in this form: $dwdZ$, means the derivative of w, the Faddeyeva function, with respect to the parameter Z. All derivatives were calculated using chain rules. Note as well that we will not explicitly write the derivatives of the HTP with respect to Δ_0 or Δ_2 since they are the same as the derivatives with respect to Γ_0 and Γ_2 except for a factor i. Finally, if the $\pm$ sign of Z is not specified, it is because the expression takes the same form whether Z_- or Z_+ is used.

$$\frac{\partial w(iZ_\pm)}{\partial Z_\pm} = 2Z_\pm w(iZ_\pm) - \frac{2}{\sqrt{\pi}} = dwdZ_\pm \tag{1}$$

$$\begin{aligned} Afactor &= \frac{\sqrt{\pi}c}{\nu_0 v_{a0}} \\ Bfactor &= \frac{v_{a0}^2\sqrt{\pi}}{2\tilde{C}_2\sqrt{Y}} \end{aligned} \tag{2}$$

$$\begin{aligned} \frac{\partial Z}{\partial \tilde{C}_0} &= \frac{1}{2\sqrt{(X+Y)}\tilde{C}_2} = dZd\tilde{C}_0 \\ \frac{\partial Z}{\partial \Gamma_0} &= \frac{1-\eta}{2\sqrt{(X+Y)}\tilde{C}_2} = dZd\Gamma_0 \end{aligned} \tag{3}$$

$$\frac{\partial Z_\pm}{\partial \nu_0} = \frac{1}{2\sqrt{X+Y}}\left(\frac{i}{\tilde{C}_2} + \frac{2Y}{\nu_0}\right) \pm \frac{1}{2\sqrt{Y}}\frac{2Y}{\nu_0} = dZ_\pm d\nu_0 \tag{4}$$

$$\frac{\partial Z_\pm}{\partial \tilde{C}_2} = \frac{1}{2\sqrt{X+Y}}\left(\frac{-X}{\tilde{C}_2} - \frac{2Y}{\tilde{C}_2}\right) \pm \frac{1}{2\sqrt{Y}}\frac{-2Y}{\tilde{C}_2} = dZ_\pm d\tilde{C}_2 \tag{5}$$

$$\frac{\partial Z_\pm}{\partial v_{a0}} = \frac{Y}{v_{a0}}\left[\frac{1}{\sqrt{X+Y}} \pm \frac{1}{\sqrt{Y}}\right] = dZ_\pm dv_{a0} \tag{6}$$

$$\begin{aligned}
\frac{\partial \tilde{C}_2}{\partial C_2} &= (1-\eta) = d\tilde{C}_2 dC_2 \\
\frac{\partial \tilde{C}_2}{\partial \eta} &= -C_2 = d\tilde{C}_2 d\eta \\
\frac{\partial \tilde{C}_0}{\partial C_2} &= -(3/2)(1-\eta) = d\tilde{C}_0 dC_2 \\
\frac{\partial \tilde{C}_0}{\partial \eta} &= -(C_0 - 3C_2/2) = d\tilde{C}_0 d\eta
\end{aligned} \tag{7}$$

Now that we have defined some basic derivatives and constants that will be re-used in the subsequent equations, we move on to the calculation of the derivatives of $A(\nu)$ and $B(\nu)$.

$$\frac{\partial A}{\partial \nu_0} = Afactor\left[-\frac{(w(iZ_-) - w(iZ_+))}{\nu_0} + dwdZ_- \times dZ_- d\nu_0 - dwdZ_+ \times dZ_+ d\nu_0\right] \tag{8}$$

$$\frac{\partial A}{\partial \Gamma_0} = Afactor\left(dwdZ_- - dwdZ_+\right) dZ d\Gamma_0 \tag{9}$$

$$\begin{aligned}
\frac{\partial A}{\partial \Gamma_2} = Afactor\Big[&dwdZ_-(dZ_- d\tilde{C}_2 \times d\tilde{C}_2 dC_2 + dZ d\tilde{C}_0 \times d\tilde{C}_0 dC_2) \\
&-dwdZ_+(dZ_+ d\tilde{C}_2 \times d\tilde{C}_2 dC_2 + dZ d\tilde{C}_0 \times d\tilde{C}_0 dC_2)\Big]
\end{aligned} \tag{10}$$

$$\frac{\partial A}{\partial \eta} = Afactor \Big[dwdZ_-(dZ_- d\tilde{C}_2 \times d\tilde{C}_2 d\eta + dZ d\tilde{C}_0 \times d\tilde{C}_0 d\eta) \\ -dwdZ_+(dZ_+ d\tilde{C}_2 \times d\tilde{C}_2 d\eta + dZ d\tilde{C}_0 \times d\tilde{C}_0 d\eta) \Big] \tag{11}$$

$$\frac{\partial A}{\partial \nu_{VC}} = Afactor\,(dwdZ_- - dwdZ_+)\,dZ d\tilde{C}_0 \tag{12}$$

$$\frac{\partial A}{\partial v_{a0}} = Afactor \left[-\frac{w(iZ_-) - w(iZ_+)}{v_{a0}} + dwdZ_- \times dZ_- dv_{a0} - dwdZ_+ \times dZ_+ dv_{a0} \right] \tag{13}$$

$$\frac{\partial B}{\partial \nu_0} = Bfactor \Big[-\frac{1}{\nu_0} \left((1 - Z_-^2) w(iZ_-) - (1 - Z_+^2) w(iZ_+) \right) \\ -2Z_- \times dZ_- d\nu_0 \times w(iZ_-) + (1 - Z_-^2) dwdZ_- \times dZ_- d\nu_0 \\ +2Z_+ \times dZ_+ d\nu_0 \times w(iZ_+) - (1 - Z_+^2) dwdZ_+ \times dZ_+ d\nu_0 \Big] \tag{14}$$

$$\frac{\partial B}{\partial \Gamma_0} = Bfactor \left[-2Z_- \times dZ d\Gamma_0 \times w(iZ_-) + (1 - Z_-^2) dwdZ_- \times dZ d\Gamma_0 \\ +2Z_+ \times dZ d\Gamma_0 \times w(iZ_+) - (1 - Z_+^2) dwdZ_+ \times dZ d\Gamma_0 \right] \tag{15}$$

$$\begin{aligned} \frac{\partial B}{\partial \Gamma_2} = & - \frac{B}{\tilde{C}_2} d\tilde{C}_2 dC2 \\ & + Bfactor \Bigg\{ \frac{1}{\tilde{C}_2} d\tilde{C}_2 dC_2 \left((1 - Z_-^2) w(iZ_-) - (1 - Z_+^2) w(iZ_+) \right) \\ & + \Big(dZ_- d\tilde{C}_2 \times d\tilde{C}_2 dC_2 + dZ d\tilde{C}_0 \times d\tilde{C}_0 dC_2 \Big) \times \left(-2Z_- w(iZ_-) + (1 - Z_-^2) dwdZ_- \right) \\ & - \Big(dZ_+ d\tilde{C}_2 \times d\tilde{C}_2 dC_2 + dZ d\tilde{C}_0 \times d\tilde{C}_0 dC_2 \Big) \times \left(-2Z_+ w(iZ_+) + (1 - Z_+^2) dwdZ_+ \right) \Bigg\} \end{aligned} \tag{16}$$

$$\begin{aligned} \frac{\partial B}{\partial \eta} = & - \frac{B}{\tilde{C}_2} d\tilde{C}_2 d\eta \\ & + Bfactor \Bigg\{ \frac{1}{\tilde{C}_2} d\tilde{C}_2 d\eta \left((1 - Z_-^2) w(iZ_-) - (1 - Z_+^2) w(iZ_+) \right) \\ & + \Big(dZ_- d\tilde{C}_2 \times d\tilde{C}_2 d\eta + dZ d\tilde{C}_0 \times d\tilde{C}_0 d\eta \Big) \times \left(-2Z_- w(iZ_-) + (1 - Z_-^2) dwdZ_- \right) \\ & - \Big(dZ_+ d\tilde{C}_2 \times d\tilde{C}_2 d\eta + dZ d\tilde{C}_0 \times d\tilde{C}_0 d\eta \Big) \times \left(-2Z_+ w(iZ_+) + (1 - Z_+^2) dwdZ_+ \right) \Bigg\} \end{aligned} \tag{17}$$

$$\frac{\partial B}{\partial \nu_{\mathrm{VC}}} = Bfactor\Big(-2Z_- \times dZd\tilde{C}_0 \times w(iZ_-) + (1-Z_-^2)dwdZ_- \times dZd\tilde{C}_0 + 2Z_+ \times dZd\tilde{C}_0 \times w(iZ_+) - (1-Z_+^2)dwdZ_+ \times dZd\tilde{C}_0\Big) \tag{18}$$

$$\begin{aligned}\frac{\partial B}{\partial v_{a0}} =& \frac{2B}{v_{a0}} + Bfactor\Big[-\frac{1}{v_{a0}}\left((1-Z_-^2)w(iZ_-) - (1-Z_+^2)w(iZ_+)\right) \\ & -2Z_- \times dZ_-dv_{a0} \times w(iZ_-) + (1-Z_-^2)dwdZ_- \times dZ_-dv_{a0} \\ & +2Z_+ \times dZ_+dv_{a0} \times w(iZ_+) - (1-Z_+^2)dwdZ_+ \times dZ_+dv_{a0}\Big]\end{aligned} \tag{19}$$

The remaining part is to get the final expressions for the entire lineshape. In order to do so, we derive the denominator of the HTP referred to has HTPd, omitting the π factor. The full expressions are not explicitly written since they all take the same form of eq. 20.

$$\frac{\partial \mathrm{HTP}}{\partial X} = \frac{\mathrm{Amp}}{\pi} \times \frac{dAdX \times \mathrm{HTPd} - A \times d\mathrm{HTPd}dX}{\mathrm{HTPd}^2} \tag{20}$$

$$\frac{\partial \mathrm{HTPd}}{\partial \nu_0} = -dAd\nu_0\left[\nu_{\mathrm{VC}} - \eta(C_0 - 3C_2/2)\right] + \frac{\eta C_2}{v_{a0}^2}dBd\nu_0 \tag{21}$$

$$\frac{\partial \mathrm{HTPd}}{\partial \Gamma_0} = -dAd\Gamma_0\left[\nu_{\mathrm{VC}} - \eta(C_0 - 3C_2/2)\right] + \eta A + \frac{\eta C_2}{v_{a0}^2}dBd\Gamma_0 \tag{22}$$

$$\frac{\partial \mathrm{HTPd}}{\partial \Gamma_2} = -dAd\Gamma_2\left[\nu_{\mathrm{VC}} - \eta(C_0 - 3C_2/2)\right] - \frac{3\eta A}{2} + \frac{\eta}{v_{a0}^2}\left(B + C_2dBd\Gamma_2\right) \tag{23}$$

$$\frac{\partial \mathrm{HTPd}}{\partial \eta} = -dAd\eta\left[\nu_{\mathrm{VC}} - \eta(C_0 - 3C_2/2)\right] + A(C_0 - 3C_2/2) + \frac{C_2}{v_{a0}^2}\left(B + \eta dBd\eta\right) \tag{24}$$

$$\frac{\partial \mathrm{HTPd}}{\partial \nu_{\mathrm{VC}}} = -dAd\nu_{\mathrm{VC}}\left[\nu_{\mathrm{VC}} - \eta(C_0 - 3C_2/2)\right] - A + \frac{\eta C_2}{v_{a0}^2}dBd\nu_{\mathrm{VC}} \tag{25}$$

$$\frac{\partial \mathrm{HTPd}}{\partial v_{a0}} = -dAdv_{a0}\left[\nu_{\mathrm{VC}} - \eta(C_0 - 3C_2/2)\right] + \frac{\eta C_2}{v_{a0}^2}\left(dBdv_{a0} - \frac{2B}{v_{a0}}\right) \tag{26}$$